# Highly stable blue light-emitting materials with a three-dimensional architecture: improvement of charge injection and electroluminescence performance†

Ting Lei,[a] Jia Luo,[a] Lei Wang,[b] Yuguo Ma,[a] Jian Wang,[b] Yong Cao*[b] and Jian Pei*[a]

Two classes of blue emitters bearing electron-rich or electron-deficient units were developed for organic light-emitting diodes. Such shape persistent three-dimensional (3D) structures provided six molecules emitting pure and stable blue light. The photophysical, electrochemical, and thermal properties as well as the thin film morphologies of these blue emitters were investigated in detail. These results indicated that the side groups did not change the photophysical properties, but significantly affected the electrochemical properties to improve the charge injection and the aggregation behaviours of the molecules. The electroluminescence performance was greatly improved without using 1,3,5-tris(N-phenylbenzimidazol-2-yl)benzene (TPBI) as an electron injection layer after the introduction of **Taz** and **Oxd** as the side groups. In comparison with **sFOMe**, 9,9′-spirobifluorene-containing compounds (**sFTaz**, and **sFOxd**) exhibited better electroluminescence due to the improvement of the electron injection ability after the introduction of electron-deficient groups. These investigations provide us with an important way to improve the OLED efficiency through the modification of the chemical structure.

## Introduction

Organic light-emitting diodes (OLEDs) have attracted considerable attention in the past two decades due to their application in full-color flat panel displays and solid-state light sources.[1] For a long time, as one of three elementary colors and good energy transfer donors, blue emitters with good stability, chromaticity, and high efficiency have been very limited.[2,3] Among blue light emitting materials, oligo- and polyfluorene derivatives (**PFs**) are the most promising candidates for OLEDs.[4] However, the formation of ketone defects or excimers/aggregates during device fabrication and operation prevents **PFs** from being excellent commercial blue emitters.[5] In contrast, spiro-linked molecules including 9,9′-spirobifluorene derivatives exhibit excellent thermal stabilities, amorphous film morphologies, increased glass-transition temperatures ($T_g$), and high quantum efficiencies for OLEDs.[6–9]

In our previous contributions,[6a–c] we designed and synthesized a three-dimensional (3D) skeleton, which was constructed by a truxene core[6d] and three spiro-linked fluorene moieties (as shown in Scheme 1). Such skeleton has two readily modifiable sites: (i) the conjugated arms, which can introduce chromophores simply through a Suzuki–Miyaura coupling reaction;[6b,c] (ii) the planar truxene core, which can be modified by various functional groups without much interference to the arms (Scheme 1). The rigid 3D structures can form excellent amorphous states to prevent the formation of the long wavelength emission induced by excimers or aggregates, and they display excellent thermal stability and good EL performance without ketone defects.[6a] Recently, we successfully applied this structure in the synthesis of a new family of highly stable small-molecular blue emitters with the fabrication of multilayer devices (ITO/PEDOT/PVK/blue emitter/TPBI/Ba/Al).[6a] However, during the operation of these devices, we observed an imbalance of the hole and electron transport in the active layer. As we know, OLEDs are "dual-injection" devices, which need holes and electrons, respectively, injected into the emission layer under an electric field.[1–3] Therefore, it is important to lower the charge injection barrier and balance their transport in the design of high performance OLED devices. To achieve high performance from our materials, poly(N-vinylcarbazole) (PVK) and 1,3,5-tris(N-phenylbenzimidazol-2-yl)benzene (TPBI) were, respectively, used as a hole and electron injection/transport layer in this device structure. Such a multilayer device complicates the fabrication, and more importantly, TPBI needs a high vacuum vapor deposition process, which greatly raises the costs and prevents their industrial application.

The strategy of chemical structure modification of the light-emitting molecule is also an efficient way to improve the charge injection. This approach can balance hole and electron transport in the emitting layer, and in the same time, reduce the complexity of devices through the incorporation of the charge transport moieties on a main chain,[9] chain ends,[10] and

[a] Beijing National Laboratory for Molecular Sciences (BNLMS) Key Labs of Bioorganic Chemistry and Molecular Engineering and of Polymer Chemistry, College of Chemistry, Peking University, Beijing 100871. E-mail: jianpei@pku.edu.cn
[b] Institute of Polymer Optoelectronic Materials and Devices, South China University of Technology, and Key Laboratory of Specially Functional Materials of Ministry of Education, Guangzhou 510640, China
† Electronic supplementary information (ESI) available: Experimental details. See DOI: 10.1039/b9nj00723g
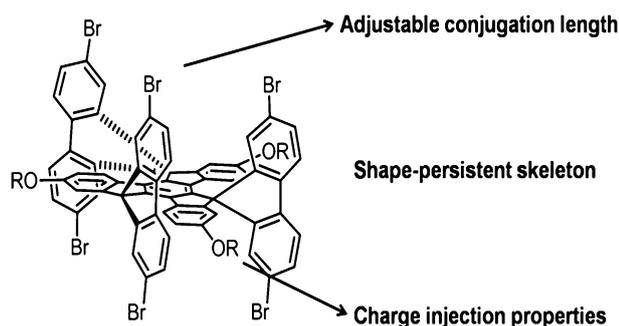
**Scheme 1** Three dimensional skeleton and our design strategy.

the side of a chain.[11] Herein, we introduced the electron-rich unit (carbazole) and electron-deficient moieties (1,2,4-triazole and 2,5-diphenyl-1,3,4-oxadiazole) to our 3D skeleton. These functional groups were widely applied in the enhancement of the charge injection and transport of light-emitting materials.[9–13] After appending with different hole or electron injection materials with flexible alkyl chains, we developed six blue light emitting materials (Scheme 2 shows the structures of compounds **sFCbz**, **sFTaz**, **sFOxd**, **FCbz**, **FTaz**, and **FOxd**) to investigate their hole or electron injection abilities and device performances. This investigation not only provides us with a way of improving the OLED efficiency through the modification of the chemical structure, but also reveals the side chain effects on the aggregation behavior of molecules and their device performances.

## Results and discussion

### Synthesis

The general synthetic routes to the six compounds are illustrated in Scheme 3. Compounds **7** and **9** were synthesized according to the literature.[11c,14] Compound **8** was obtained by treating commercially available 1,2,4-triazole with DBU (1,8-diazabicyclo[5.4.0]undec-7-ene) and 1,6-dibromohexane in THF. For the synthesis of target molecules, **sFOMe** or **FOMe** [6a] was first treated with BBr$_3$ and then subjected to an alkylation reaction with **7**, **8**, or **9** to afford the six blue emitters in yields of 80–90%. These compounds showed good solubility in common solvents, such as CH$_2$Cl$_2$, THF, toluene, and dimethylformamide (DMF). Molecular modeling indicated that **sFCbz** exhibited a highly rigid skeleton appended with three "antenna" groups, which was helpful for carrier injection (Fig. S1†).[12d]
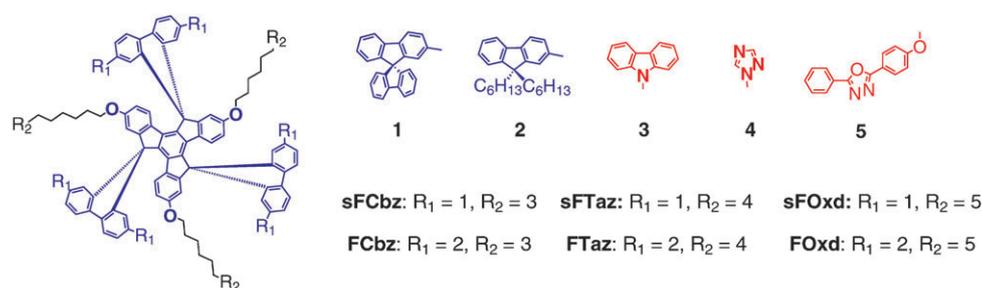
### Thermal properties

The thermal properties of the six emitters were investigated by thermogravimetric analysis (TGA) and differential scanning calorimetry (DSC). All six compounds exhibit excellent thermal stabilities, and the 5% weight loss occurring from 330 °C to 425 °C indicates that the side chains have sufficient thermal stabilities. DSC results showed that **sFCbz**, **sFTaz**, and **sFOxd** exhibited no glass transition temperatures ($T_g$) or melting points from 25 to 350 °C. The results are consistent with our previous results for **sFOMe** and **FOMe**. In contrast, the obvious melting peaks were observed to be at around 294 °C for **FCbz**, 290 °C for **FTaz**, and 252 °C for **FOxd** after introducing the side chains (Fig. S5†). This result suggests that although the side chains usually do not affect the photophysical properties (*vide infra*), the aggregation behavior can be significantly changed.

### Photophysical properties

Fig. 1 shows the UV-vis absorption and photoluminescence (PL) of three compounds based on 9,9′-spirobifluorenes (**sFCbz**, **sFTaz**, and **sFOxd**). These compounds showed almost identical absorptions and PL features with **sFOMe** both in solution and solid state.[6a] The main absorption peaks at 350 nm are assigned to the conjugated arm π–π* transitions and the extinction coefficients are more than 10$^5$. The PL maximum $\lambda_{max}$ of **sFCbz**, **sFTaz**, and **sFOxd** in the solid state shows merely about 10 nm red-shifts relative to that of dilute solutions. These results indicate that the conjugated arms of the main skeleton are not affected by the various side groups because of the non-conjugated manner of linking. It also demonstrates that the shape-persistent 3D structure can efficiently reduce the intermolecular π–π interactions. The arising shoulder of the absorption spectra of **sFOxd** around 310 nm can be attributed to the absorption of the oxadiazole segments,[10a,b] and the emission of these segments does not affect the PL spectra whether in solution or in solid state. As indicated in Table 1, there is a good match of the emission of the **Oxd** units and the absorption of the conjugated arms, which meets the requirement of the Förster energy transfer.[15] When excited at 310 nm, the PL spectrum shows the same emission as when excited at 348 nm whether in dilute solution or in solid state. This complete quenching of the emission of **Oxd** indicates an efficient intramolecular energy transfer between the side groups and the conjugated arms (Fig. S3†).[10a] **FCbz**, **FTaz**, and **FOxd** based on 9,9-dihexylfluorene also did not exhibit obvious changes compared with **FOMe**, and



**Scheme 2** The structures of the six 3D blue emitters.

**sFOMe**: $R_1$=2
**FOMe**: $R_1$=3

**sFOH**: $R_1$=2
**FOH**: $R_1$=3

**7**    **8**    **9**
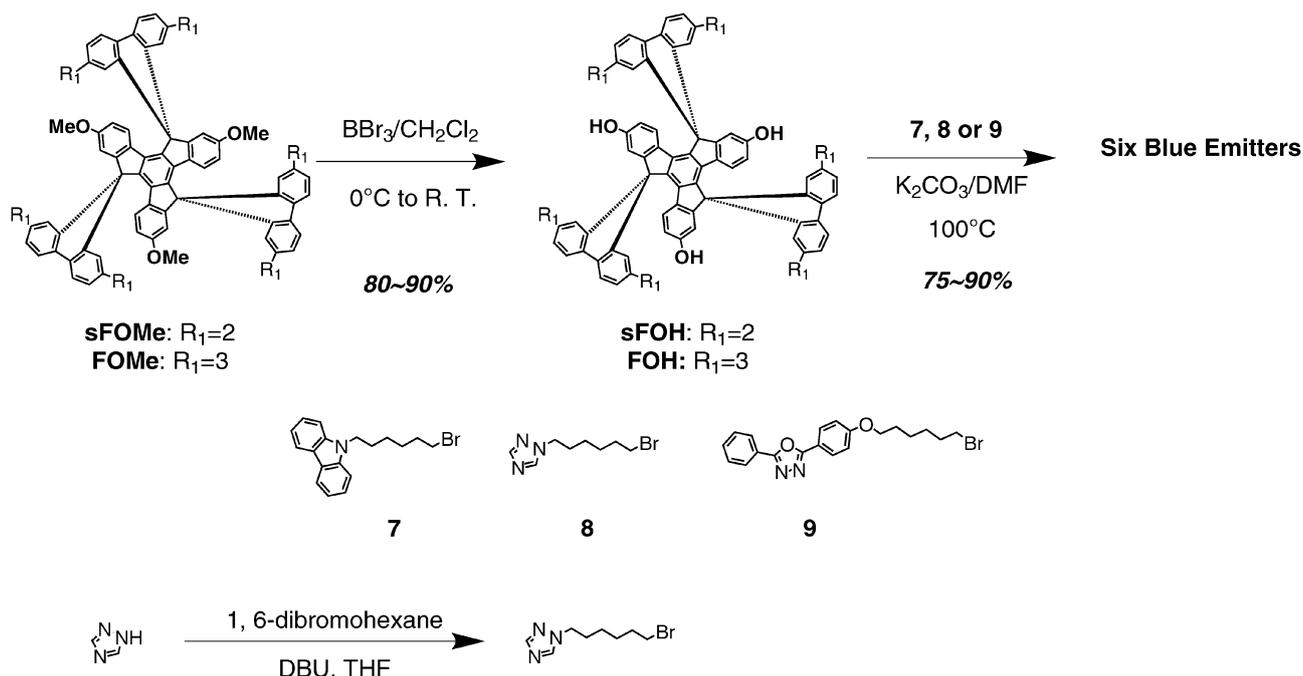
**Scheme 3**    Synthetic routes to the six blue emitters.

display similar changes to **sFCbz**, **sFTaz**, and **sFOxd** (Fig. S2). These results support our assumption that the decreased solubility and changed morphology (*vide infra*) of **FCbz**, **FTaz**, and **FOxd** are caused by the interaction of the side chain and alkyl chains, not by the interaction with the conjugated arms. Table 1 summarizes the photophysical properties of the six blue emitters.

### Electrochemical properties in thin film

We employed cyclic voltammetry (CV) to investigate the electrochemical properties of the six emitters in thin films and to estimate the energy levels of their highest occupied molecular orbital (HOMO) and lowest unoccupied molecular orbital (LUMO). The measurements were performed by drop-casting the THF solutions of the compounds on a glassy carbon electrode in an electrolyte of 0.1 M *n*-Bu$_4$NPF$_6$ in acetonitrile using Ag/AgCl (4.6 eV below the vacuum level) as

the reference electrode. The HOMO and LUMO levels in the solid states were estimated by the onset of the oxidation and the reduction processes ($E_{HOMO} = -E_{ox} -4.6$ eV, $E_{LUMO} = -E_{re} -4.6$ eV). As shown in Fig. 2, the HOMO levels of **sFCbz**, **sFTaz**, and **sFOxd** exhibited almost identical values at *ca.* $-5.6$ eV. However, their LUMO levels were quite different (for **sFCbz**, $E_{LUMO} = -2.4$ eV; **sFTaz**, $E_{LUMO} = -2.7$ eV; **sFOxd**, $E_{LUMO} = -2.6$ eV). In consideration of the unchanged photophysical properties, this result was not caused by the central chromophores, which indicated that the introduction of the electron withdrawing groups might lower the LUMO levels of the desired compound. Additionally, the LUMO level of 2-(4-biphenyl)-5-(4-*tert*-butylphenyl)-1,3,4-oxadiazole (PBD) is close to our result.[16] Therefore, we rationally ascribed the observed LUMO levels to the LUMO of the side electron-deficient moieties. Similar phenomena were also observed in **FCbz**, **FTaz**, and **FOxd**.[10a] However, the HOMO
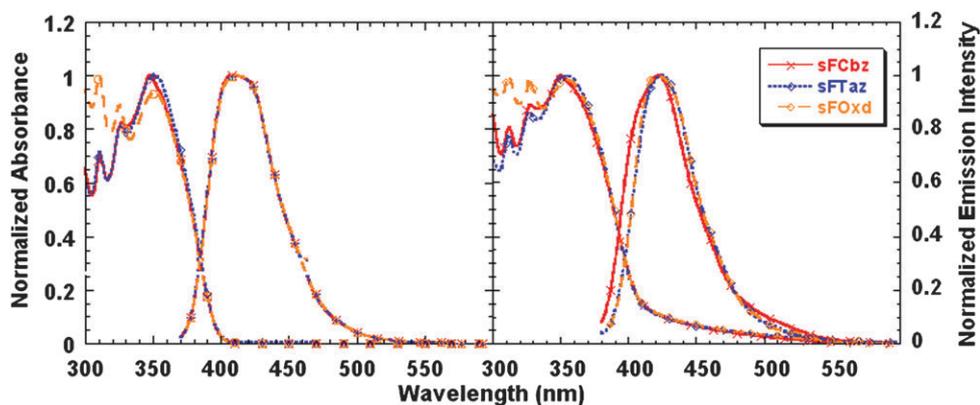


**Fig. 1** The normalized absorption and PL spectra of **sFCbz**, **sFtaz**, and **sFOxd**: (a) in dilute toluene solutions (1 × 10$^{-6}$ M); (b) in solid state (spin casting from toluene).

**Table 1** Photophysical and electrochemical properties of the six compounds

| Compds | $\lambda_{abs}$/nm (log $\varepsilon$) (Toluene) | $\lambda_{abs}$/nm (Film)[a] | $\lambda_{PL}$/nm (Toluene) | $\lambda_{PL}$/nm (Film)[a] | HOMO/eV (Film)[b] | LUMO/eV (Film)[b] |
|---|---|---|---|---|---|---|
| **sFCbz** | 348 (5.35) | 351 | 408 | 423 | −5.6 | −2.4 |
| **sFTaz** | 351 (5.34) | 355 | 411 | 425 | −5.6 | −2.6 |
| **sFOxd** | 351 (5.33), 325 (5.30) | 355 | 411 | 421 | −5.6 | −2.7 |
| **FCbz** | 347 (5.00) | 349, 327 | 407 | 423 | −5.8 | −2.3 |
| **FTaz** | 349 (4.95) | 345, 327 | 407 | 421 | −5.9 | −2.5 |
| **FOxd** | 348 (5.52), 327 (5.53) | 348, 327 | 403, 418 | 425 | −5.9 | −2.5 |

[a] Spin-cast from toluene solution (5 mg mL$^{-1}$). [b] Drop-cast from THF solution (2 mg mL$^{-1}$).

level of **sFCbz** does not show much change, which can be explained by the small difference between the HOMO level of carbazole ($E_{HOMO}$ = −5.5 eV)[12d] and the conjugated arms ($E_{HOMO}$ = −5.6 eV). **FCbz**, **FTaz**, and **FOxd** also show similar trends of the movement of LUMO levels, however, the HOMO and LUMO levels of **FCbz**, **FTaz**, and **FOxd** exhibit some differences comparing with the **sF** series, which might attributed to the greatly changed film morphologies (*vide infra*). (Fig. S4,† Table 1).

### Surface morphology of thin film

Inspired by the DSC results, we further investigated the film morphologies of **sFCbz**, **sFTaz**, **sFOxd**, **FCbz**, **FTaz**, and **FOxd** by tapping-mode atomic force microscopy (TM-AFM). Fig. 3 shows the height and phase images of **sFTaz** and **FTaz** in thin film spin-cast on a quartz plane. As shown by the height image, the **sFTaz** film displays a neat film with roughness lower than 10 nm; in contrast, the **FTaz** film has a roughness greater than 50 nm and many crystalline domains. AFM phase imaging is more sensitive to the composition, friction, and grain edges of the sample. As indicated by the phase image, **sFTaz** formed a uniform and homogenous film; however, the **FTaz** film was inhomogeneous and displayed some highlighted edges and small zones, which can be attributed to the partial crystallization of the film. This phenomenon also existed in the **Cbz** and **Oxd** substituted counterparts (Fig. S7†). Considering the DSC results, we can conclude that the side chains significantly affect the aggregation of **FCbz**, **FTaz**, and **FOxd**, and result in different film morphologies. Therefore, the investigation of the OLED
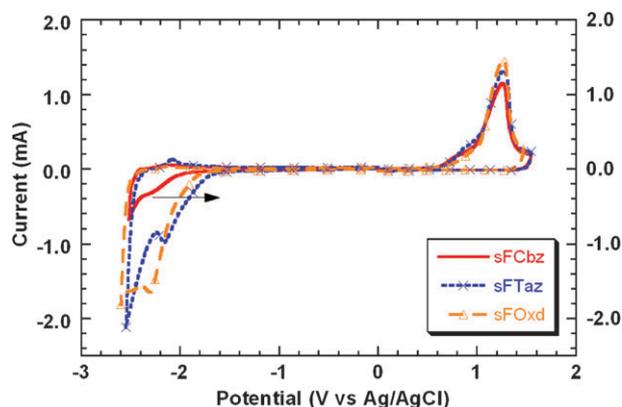
device performance was only carried out using **sFCbz**, **sFTaz**, and **sFOxd**.

### Electroluminescence properties and OLED performances

To further investigate the effects of the side chains, single-layer and double-layer OLED devices were fabricated. First, we fabricated single layer devices with a configuration of ITO/PEDOT (40 nm)/EL (60 nm)/Ba (4 nm)/Al (150 nm), which reflected the intrinsic charge injection/transport abilities of the emissive layer (Fig. 4a). The luminescence efficiencies (LE) of **sFCbz**, **sFTaz**, and **sFOxd** are much better than their parent compound **sFOMe** (0.01 cd A$^{-1}$). This improvement can be rationally attributed to the introduction of the side chains (Table 2). **sFTaz** and **FTaz** showed the best luminous efficiency up to 0.1 cd A$^{-1}$ with the single layer device configuration. The current density–voltage (J–V) characteristics were also investigated to illustrate the device performance. As shown in Fig. 5a, all the devices were turned on at low voltages around 5.0 V. Compared with the current density of the **sFOMe** device, those of the devices fabricated with **sFCbz** show little change; in contrast, the current densities of **sFTaz** and **sFOxd** are clearly lowered. These results indicated that the introduction of the **Cbz** groups did not apparently change the transport of the charge carriers, and in the case of **sFTaz** and **sFOxd**, the transport of holes and electrons becomes more balanced, which resulted in an increase of the recombination and efficiencies. Therefore, electrons were considered as the minor carriers in skeleton **sFOMe** and the introduction of



**Fig. 2** Cyclic voltammograms of drop casting films of **sFCbz**, **sFtaz**, and **sFOxd**. Scan rate, 100 mV s$^{-1}$; working electrode, glassy carbon; auxiliary electrode, Pt wire; reference electrode, Ag/AgCl; supporting electrolyte *n*-Bu$_4$NPF$_6$ (0.1 M, CH$_3$CN).
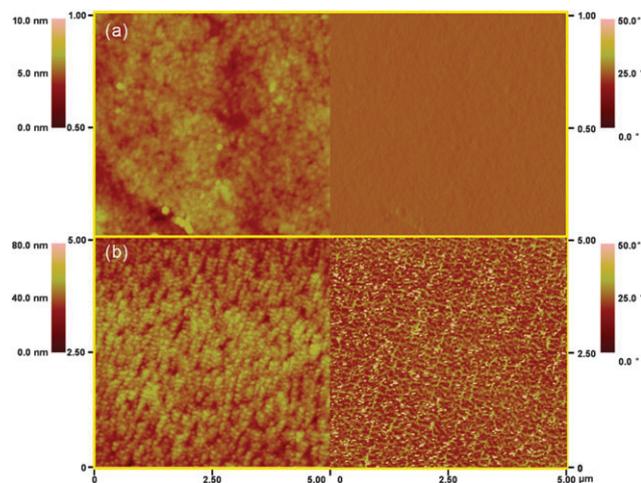


**Fig. 3** TM-AFM height images and phase images of (a) **sFTaz** (1 × 1 μm), (b) **FTaz** (5 × 5 μm) in thin film (spin-cast on a quartz plane from 5 mg mL$^{-1}$ toluene solution).

This journal is © The Royal Society of Chemistry and the Centre National de la Recherche Scientifique 2010
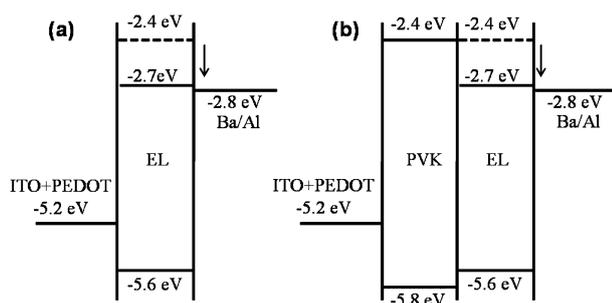
**Fig. 4** Energy level scheme for (a) single-layer device; (b) double-layer device. EL level was estimated according to the CV data. The LUMO energy level was lowered from $-2.4$ eV (**sFOMe**, dashed line)[6a] to $-2.7$ eV (**sFTaz**, solid line).

electron-deficient units can lead to the increase of electron injection/transport by lowering the electron injection barrier (Fig. 4). Importantly, the substitutions only occurred at the planar truxene moiety, which leads to the preservation of the maximum effective conjugated length and similar optical spectra to their parent compound **sFOMe**. Hence, the EL chromatic coordinates (CIE 1931) of all compounds proved them promising pure blue emitters (Table 2).

On the other hand, PVK (HOMO $-5.8$ eV)[17] was introduced as a hole transporting layer or an electron blocking layer to build double-layer devices with the configuration of ITO/PEDOT (40 nm)/PVK (40 nm)/EL (60 nm)/Ba (4 nm)/Al (150 nm) (as shown in Fig. 4b). The uniform polymer layer
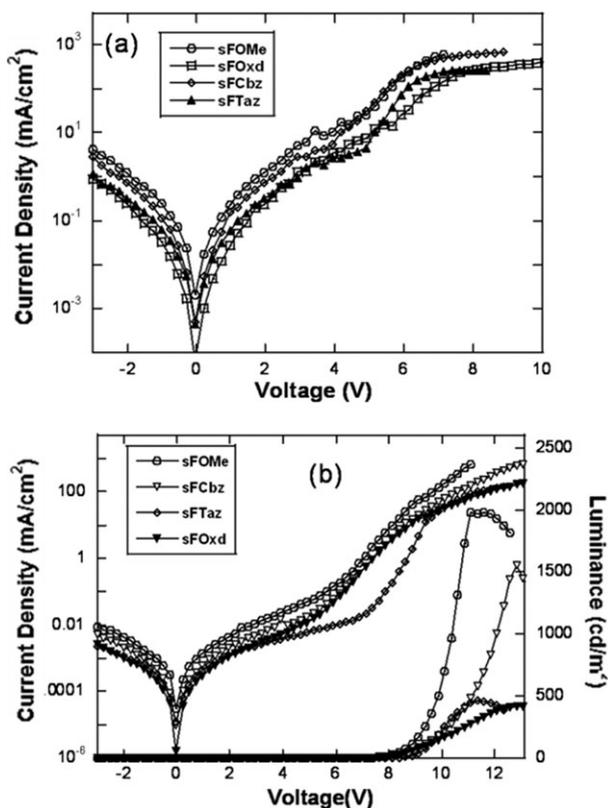




**Fig. 5** (a) *J–V* characteristics of single layer devices with structure: ITO/PEDOT/EL/Ba/Al; (b) *J–V–L* Characteristics of the double layer devices with structure **2**: ITO/PEDOT/PVK/EL/Ba/Al.

of PVK can also effectively decrease the leakage current.[18] By this configuration, although the turn-on voltage increases by *ca.* 1.5–3 V, the maximum efficiency can also reach 0.39–0.80 cd A$^{-1}$. As shown in Table 3, the **Cbz** substituted blue emitter gives a small improvement in LE (0.04 cd A$^{-1}$) relative to **sFOMe**, while the other two exhibited increased efficiency of 0.17 cd A$^{-1}$ for **sFOxd** and 0.41 cd A$^{-1}$ for **sFTaz**. Therefore, we can conclude that the electron-deficient groups are much better for our structure to improve the device performance. This result is caused by the increased electron injection by the electron-deficient group. In the density–voltage–luminance (*J–V–L*) characteristics (Fig. 5b), the current density of **sFTaz** was an order of magnitude lower than that of **sFOMe**, but the luminous efficiency remained at a higher level. Compared to the single-layer devices, double-layer devices showed much lower current density, which can be attributed to the decreased leakage current and the balanced charge carrier injection. The **Taz** unit substituted molecule exhibited a more obvious enhancement than that of **Oxd**, which is consistent with the previous literature.[13] Thus, **Taz** is a better group for this system, and this may be explained by its much lowered LUMO levels. The current density–luminous efficiency (*J*–LE) curve demonstrates the trend in LE as the current density increases. Stable luminous efficiency was obtained in the device fabricated with **sFCbz** as well as that with **sFOMe** (Fig. S8†). The results showed that the hole and electron recombination was disturbed at high operation current densities for **sFOxd** and **sFTaz**.

The electroluminescence spectra recorded for the double-layer devices reveals three similar main emission peaks for all emitters, two very sharp peaks at *ca.* 412 nm and *ca.* 428 nm and one much broader centered around 460 nm (Fig. 6a). Moreover, the emission $\lambda_{max}$ is similar to that of their PL spectra. All the devices showed blue light with chromatic coordinates (CIE 1931) in a range of (0.17–0.18, 0.07–0.10). Importantly, as the operation voltage increased in a rational range, the EL intensity of all the devices was enhanced but the shape and emission wavelength remained unchanged as well as the chromatic coordinates, which proved the optical spectrum stability under an electric field (Fig. 6b, Fig. S9†). Additionally, for all the compounds, the PL efficiencies of the films were measured by integrating a sphere system before and after annealing at 150 °C under nitrogen atmosphere. Although the PL efficiencies in thin film did not show much increase (Table 2), the device performances obtained a small improvement (10–20%) for double-layer devices. This can be attributed to the optimization of the interface characteristic and the film morphologies, which leads to the minimized crystal interface and the improved film conductivity.[19]

## Conclusion

Six new three-dimensional blue emitters bearing electron-rich (**Cbz**), or electron-deficient (**Taz** and **Oxd**) groups have been developed for organic light-emitting diodes. The investigation of their photophysical properties showed that such 3D skeleton can be orthogonally modified without affecting the conjugated arms. Electrochemical results directly demonstrate the side chain effect on the HOMO and LUMO levels. Especially, the

**Table 2** Device performance with the single-layer: ITO/PEDOT/ EL/Ba/Al

| Compds | $V_{on}/V$ | $L_{max}/cd\ m^{-2}$ | $LE_{max}/cd\ A^{-1}$ | CIE 1931($x$, $y$) | $\Phi_{film}$ | $\Phi'_{film}{}^a$ |
|---|---|---|---|---|---|---|
| **sFCbz** | 4.7 | 230 | 0.04 | 0.20, 0.21 | 0.22 | 0.39 |
| **sFTaz** | 5.2 | 150 | 0.10 | 0.17, 0.12 | 0.21 | 0.19 |
| **sFOxd** | 5.2 | 250 | 0.08 | 0.17, 0.11 | 0.19 | 0.22 |

$^a$ Measured after annealing at 150 °C under nitrogen atmosphere.

introduction of the electron-deficient groups can obviously lower the LUMO levels of the molecules, which can help the injection of the electron from the anode. However, thermal properties and AFM results show that the enhanced side interaction of **FCbz**, **FTaz**, and **FOxd** changed its film morphologies; in contrast, **sFCbz**, **sFTaz**, and **sFOxd** exhibit much better thermal stabilities and film morphologies. The single-layer device results proved the improvement of the electron injection abilities, and the double-layer devices exhibit largely improved efficiencies after the introduction of **Taz** and **Oxd** side groups. Although this molecule only exhibited moderate device performances, we have demonstrated this way of improving the device efficiency through chemical modification is indeed effective. To further improve device performances using **sFCbz**, **sFTaz**, or **sFOxd** as the active materials, we are currently investigating molecules modified with different types and numbers of side groups and their device performances.

## Experimental

### General methods

Chemicals were purchased and used as received. All air and water sensitive reactions were performed under nitrogen atmosphere. Toluene and tetrahydrofuran (THF) were distilled from sodium and benzophenone ketyl. $^1H$ and $^{13}C$ NMR spectra were recorded on a Varian Mercury plus 300 MHz and Bruker ARX-400 (400 MHz) using CDCl$_3$ as solvent. All chemical shifts were reported in parts per million (ppm), $^1H$ NMR chemical shifts were referenced to TMS (0 ppm) or CHCl$_3$ (7.26 ppm), and $^{13}C$ NMR chemical shifts were referenced to CDCl$_3$ (77.00 ppm). Absorption spectra were recorded on a PerkinElmer Lambda 35 UV-vis Spectrometer. PL spectra were carried out on a PerkinElmer LS55 Luminescence Spectrometer. MALDI-TOF mass spectra were recorded on a Bruker BIFLEX III time-of-flight (TOF) mass spectrometer (Bruker Daltonics, Billerica, MA, USA) using a 337 nm nitrogen laser with dithranol as matrix. Elemental analyses were performed using a German Vario EL III elemental analyzer. Thermal gravity analyses (TGA) were carried out on a TA Instrument Q600 analyzer and differential scanning calorimetry analyses were performed on a METTLER TOLEDO Instrument



**Fig. 6** (a) Normalized electroluminescence spectra for double-layer devices. (b) Electroluminescence spectra of devices at various driving voltages of the double-layer device: ITO/PEDOT/PVK/**sFTaz**/Ba/Al.

DSC822 calorimeter. Cyclic voltammetry was performed using a BASI Epsilon workstation and measurements were carried out in acetonitrile containing 0.1 M $n$Bu$_4$NPF$_6$ as a supporting electrolyte. A carbon electrode was used as a working electrode and a platinum wire as a counter electrode; all potentials were recorded *versus* Ag/AgCl (3M NaCl (aq.)) as a reference electrode. The scan rate was 100 mV s$^{-1}$. Atomic force microscopy studies were performed with a Nanoscope IIIa microscope (Extended Multimode, Digital Instruments, Santa Barbara, CA). All experiments were carried out in tapping mode at ambient temperature. A silicon nitride cantilever (Budget Sensors Tap300Al) was used with a resonant frequency around 300 kHz. The absolute photoluminescence efficiencies of compounds in film were measured in an integrating sphere

**Table 3** Device performance with structure double-layer: ITO/PEDOT/PVK/EL/Ba/Al

| Compds | $V_{on}/V$ | $L_{max}/cd\ m^{-2}$ | $LE_{max}/cd\ A^{-1}$ | $\lambda_{max}/nm$ | CIE 1931($x$, $y$) |
|---|---|---|---|---|---|
| **sFOMe** | 6.9 | 1980 | 0.39 | 426 | 0.17, 0.07 |
| **sFCbz** | 6.9 | 1550 | 0.43 | 426 | 0.18, 0.10 |
| **sFTaz** | 8.1 | 463 | 0.80 | 428 | 0.17, 0.08 |
| **sFOxd** | 6.6 | 414 | 0.56 | 430 | 0.17, 0.07 |

This journal is © The Royal Society of Chemistry and the Centre National de la Recherche Scientifique 2010

system (IS-080, Labsphere) under excitation from the 325 nm line of a HeCd laser.

### Device fabrication and characterization

LED was fabricated on pre-patterned indium-tin oxide (ITO) with sheet resistance 10–20 $\Omega$/square. The substrate was ultrasonically cleaned with acetone, detergent, deionized water, and 2-propanol. Oxygen plasma treatment was performed for 10 min as the final step of substrate cleaning to improve the contact angle just before film coating. Onto the ITO glass was spin-coated a layer of PEDOT:PSS film with thickness of 50 nm from its aqueous dispersion, aiming to improve the hole injection and to avoid the possibility of leakage. The PEDOT:PSS film was dried at 200 °C for 10 min. The solutions of all materials in $p$-xylene were prepared in a nitrogen-filled drybox and spin-coated on top of the ITO/PEDOT:PSS surface. Typical thickness of the emitting layer was 50–80 nm. Then a thin layer of barium as an electron injection cathode and the subsequent 200 nm thick aluminium protection layers were thermally deposited by vacuum evaporation through a mask at a base pressure below $2 \times 10^{-4}$ Pa. The deposition rate and the thickness of the barium and aluminium layers were monitored by a thickness/rate meter. The cathode area defines the active area of the device. The typical active area of the devices in this study is 0.15 cm$^2$. The EL layer spin coating process and the device performance tests were carried out within a glovebox with nitrogen circulation. The luminance of the device was measured with a calibrated photodiode. External quantum efficiency was verified by the measurement of the integrating sphere, and luminance was calibrated after the encapsulation of devices with UV-curing epoxy and thin cover glass.

### Synthesis

**sFOMe** and **FOMe** were synthesized according to our previous report.[6]

### 1-(6-Bromohexyl)-1$H$-1,2,4-triazole (8)

To a stirred suspension of 1,2,4-triazole (1.00 g, 0.0144 mol) and 1,6-dibromohexane (10.6 g, 0.0435 mol) in THF (30 mL) was added DBU (2.19 g, 0.0144 mol) $via$ syringe pump. After at room temperature for 24 h, the mixture was filtered and the cake was washed with THF (50 mL). After the filtrate was concentrated, the residue was purified by silica gel chromatography (eluent: EtOAc) to give a colorless oil. Yield: 50%. $^1$H NMR (CDCl$_3$, 300 MHz, ppm): $\delta$ 8.07 (1H, s), 7.95 (1H, s), 4.16–4.21 (2H, m), 3.38–3.42 (2H, m), 1.83–1.95 (4H, m), 1.47–1.52 (2H, m), 1.32–1.36 (2H, m). $^{13}$C NMR (CDCl$_3$, 75 MHz, ppm): $\delta$ 152.1, 143.0, 49.6, 33.7, 32.5, 29.8, 27.6, 25.8. EI-MS: $m/z$ 231.0 (M$^+$ − 1), 233.0 (M$^+$ + 1), which is 100%.

### General procedures for sFOH and FOH

To a solution of **sFOMe** or **FOMe** (0.1 mmol) in dry CH$_2$Cl$_2$ was added dropwise BBr$_3$ (0.6 mmol) under cooling in an ice bath. The mixture was stirred at room temperature for 8 h and then saturated NaHCO$_3$ aqueous was added. The aqueous layer was extracted with CH$_2$Cl$_2$. The combined extracts were dried over MgSO$_4$. After removal of solvents under reduced

pressure, the residue was purified $via$ chromatography over silica gel to afford a white solid.

**sFOH** (eluent: CH$_2$Cl$_2$) (Yield: 90%): $^1$H NMR (CDCl$_3$, 400 MHz, ppm): $\delta$ 7.85–7.81 (m, 12H), 7.68–7.66 (d, $J$ = 8.4 Hz, 6H), 7.60–7.58 (d, $J$ = 8.0 Hz, 6H), 7.41–7.39 (d, $J$ = 7.5 Hz, 6H), 7.33–7.20 (m, 30H), 7.05–6.93 (m, 30H), 6.71–6.69 (m, 18H), 6.30–6.27 (d, $J$ = 8.5 Hz, 3H), 5.90–5.87 (dd, $J$ = 8.5 Hz, $J$ = 2.4 Hz, 3H), 5.704–5.698 (d, $J$ = 2.4 Hz, 3H), 4.14 (s, 3H). $^{13}$C NMR (CDCl$_3$, 100 MHz, ppm): $\delta$ 154.8, 149.5, 149.4, 149.3, 148.7, 148.5, 141.7, 141.0, 140.7, 140.5, 140.3, 128.1, 127.9, 127.84, 127.76, 126.8, 124.11, 124.06, 122.5, 120.5, 120.4, 120.3, 119.9, 114.0, 109.3, 66.6, 66.0. MALDI-TOF MS: Calcd for C$_{213}$H$_{120}$O$_3$: 2726.93. Found: 2727.2 (M$^+$).

**FOH** (eluent: CH$_2$Cl$_2$–PE = 3 : 1) (Yield: 88%): $^1$H NMR (CDCl$_3$, 400 MHz, ppm): $\delta$ 8.11–8.09 (d, $J$ = 7.8 Hz, 6H), 7.72–7.70 (d, $J$ = 7.8 Hz, 6H), 7.57 (s, 6H), 7.42 (s, 6H), 7.30–7.20 (m, 24H), 6.91–6.88 (m, 6H), 6.60–6.58 (d, $J$ = 8.4 Hz, 3H), 6.15–6.13 (dd, $J$ = 8.4 Hz, $J$ = 2.4 Hz, 3H), 6.02 (s, 3H), 4.33 (s, 3H), 1.00–0.86 (m, 36H), 0.86–0.84 (m, 24H), 0.71–0.56 (m, 54H), 0.52–0.48 (t, $J$ = 7.5 Hz, 18H). $^{13}$C NMR (CDCl$_3$, 100 MHz, ppm): $\delta$ 154.9, 152.5, 151.4, 150.7, 149.6, 141.8, 141.7, 140.51, 140.47, 140.4, 139.7, 137.57, 131.6, 127.5, 127.0, 126.8, 125.7, 122.6, 121.8, 121.1, 120.7, 120.5, 120.2, 114.2, 109.5, 66.9, 55.1, 40.5, 40.3, 31.2, 31.0, 29.51, 29.48, 23.7, 23.5, 22.4, 22.3, 13.9, 13.7. MALDI-TOF MS: Calcd for C$_{213}$H$_{228}$O$_3$: 2835.78. Found: 2836.1 (M$^+$).

### General procedures for sF series and F series

To a mixture of **sFOH** or **FOH** (0.05 mmol) and **8** or **9** or **10** (0.20 mmol) in aqueous DMF, K$_2$CO$_3$ (0.40 mmol) were added under nitrogen atmosphere. The mixture was stirred at 100 °C. After 8 h, the mixture was cool to room temperature and poured into water. The aqueous layer was extracted three times with dichloromethane. The combined extracts were dried over MgSO$_4$. After removal of solvents under reduced pressure, the residue was purified $via$ chromatography over silica gel.

**sFCbz**, white solid, (eluent: CH$_2$Cl$_2$–PE = 1 : 1), (Yield: 72%): $^1$H NMR (CDCl$_3$, 300 MHz, ppm): $\delta$ 8.08–8.05 (d, $J$ = 8.1 Hz, 6H) 7.85–7.82 (m, 12H), 7.75–7.73 (d, $J$ = 7.8 Hz, 6H), 7.58–7.55 (d, $J$ = 8.1 Hz, 6H), 7.40–7.15 (m, 42H), 7.09–6.93 (m, 36H), 6.77–6.72 (m, 18H), 6.36–6.33 (d, $J$ = 8.7 Hz, 3H), 5.98–5.96 (d, $J$ = 8.7 Hz, 3H), 5.76 (s, 3H), 4.17–4.12 (t, $J$ = 6.9 Hz, 6H), 3.38–3.37 (t, 6H), 1.70–1.68 (m, 6H), 1.34–1.18 (m, 18H). $^{13}$C NMR (CDCl$_3$, 75 MHz, ppm): $\delta$ 158.6, 152.0, 149.9, 149.6, 149.4, 148.9, 148.8, 142.0, 141.95, 141.85, 141.2, 141.17, 141.0, 140.7, 140.5, 137.3, 131.2, 128.1, 127.9, 127.4, 126.9, 125.8, 125.3, 124.4, 124.3, 124.2, 123.0, 122.7, 121.7, 120.7, 120.6, 120.5, 120.2, 118.9, 112.5, 108.8, 67.3, 66.9, 66.2, 43.0, 29.1, 28.8, 27.0, 25.8. MALDI-ICR HR-MS: Calcd for C$_{267}$H$_{177}$N$_3$O$_3$: 3472.37845. Found: 3472.39403 (M$^+$).

**sFTaz**, white solid, (eluent: CH$_2$Cl$_2$–Acetone = 3 : 1), (Yield: 80%): $^1$H NMR (CDCl$_3$, 400 MHz, ppm): $\delta$ 7.93–7.83 (m, 18H) 7.78–7.76 (d, $J$ = 8.0 Hz, 6H), 7.60–7.50 (d, $J$ = 8.0 Hz, 6H), 7.41–7.27 (m, 30H), 7.20 (s, 6H), 7.09–6.97 (m, 30H), 6.77–6.75 (d, $J$ = 7.5 Hz, 2H), 6.75–6.72 (m, 12H), 6.35–6.33 (d, $J$ = 8.7 Hz, 3H), 5.99–5.96 (dd, $J_1$ = 8.7 Hz,

$J_2$ = 2.3 Hz, 3H), 5.755–5.761 (d, $J$ = 2.3 Hz, 3H), 4.02–3.98 (t, $J$ = 7.1 Hz, 6H), 3.38–3.37 (t, $J$ = 6.0 Hz, 6H), 1.75–1.68 (m, 6H), 1.38–1.35 (m, 6H), 1.14–1.11 (m, 12H). $^{13}$C NMR (CDCl$_3$, 100 MHz, ppm): 158.4, 151.82, 151.76, 149.7, 149.5, 149.1, 148.7, 148.6, 141.8, 141.7, 141.6, 141.99, 141.96, 140.7, 140.5, 131.0, 128.1, 127.9, 127.7, 127.2, 126.7, 125.0, 124.14, 124.06, 124.02, 122.4, 121.5, 120.5, 120.4, 120.3, 120.0, 112.3, 108.6, 67.0, 66.7, 66.0, 53.4, 49.5, 29.5, 28.8, 26.0, 25.3. MALDI-ICR HR-MS: Calcd for C$_{237}$H$_{159}$N$_9$O$_3$: 3178.25604. Found: 3178.26862 (M$^+$).

**sFOxd**, white solid, (eluent: CH$_2$Cl$_2$–ethyl acetate = 20 : 1), (Yield: 85%): $^1$H NMR (CDCl$_3$, 400 MHz, ppm): δ 8.14–8.12 (dd, $J$ = 7.3 Hz, $J$ = 2.4 Hz, 6H), 8.05–8.03 (d, $J$ = 8.8 Hz, 6H), 7.86–7.81 (m, 12H) 7.78–7.76 (d, $J$ = 8.0 Hz, 6H), 7.60–7.58 (d, $J$ = 8.0 Hz, 6H), 7.54–7.52 (m, 9H), 7.41–7.29 (m, 24H), 7.22 (s, 6H), 7.07–6.96 (m, 36H), 6.77–6.75 (d, $J$ = 7.6 Hz, 2H), 6.75–6.72(m, 12H), 6.36–6.34 (d, $J$ = 8.7 Hz, 3H), 6.01–5.99 (dd, $J_1$ = 8.7 Hz, $J_2$ = 2.3 Hz, 3H), 5.784–5.778 (d, $J$ = 2.3 Hz, 3H), 3.92–3.88 (t, $J$ = 6.5 Hz, 6H), 3.43 (s, 6H), 1.68–1.64 (m, 6H), 1.42–1.43 (m, 6H), 1.31–1.22 (m, 12H). $^{13}$C NMR (CDCl$_3$, 100 MHz, ppm): 164.6, 164.1, 161.9, 158.4, 151.8, 149.7, 149.5, 149.2, 148.7, 148.6, 141.8, 147.7, 141.6, 141.0, 140.8, 140.5, 137.1, 131.5, 131.0, 129.0, 128.6, 128.1, 127.9, 127.8, 127.7, 127.2, 126.8, 126.7, 124.15, 124.08, 124.0, 122.5, 121.5, 120.5, 120.4, 120.3, 120.0, 116.2, 114.9, 112.2, 108.7, 29.7, 29.0, 28.8, 25.7, 25.6. MALDI-TOF MS: Calcd for C$_{273}$H$_{180}$N$_6$O$_9$: 3687.39. Found: 3688.2 (M + H)$^+$.

**FCbz**, white solid, (eluent: CH$_2$Cl$_2$–PE = 1 : 4), (Yield: 73%): $^1$H NMR (CDCl$_3$, 300 MHz, ppm): δ 8.10–8.04 (m, 12H), 7.71–7.68 (d, $J$ = 6.9 Hz, 6H), 7.57 (s, 6H), 7.42 (s, 6H), 7.38–7.36 (d, $J$ = 6.9 Hz, 6H), 7.32–7.15 (m, 36H), 7.03–7.01 (d, $J$ = 7.5 Hz, 6H), 6.91–6.87 (m, 6H), 6.65–6.62 (d, $J$ = 8.4 Hz, 3H), 6.22–6.19 (dd, $J$ = 8.4 Hz, $J$ = 2.4 Hz, 3H), 6.10–6.09 (d, $J$ = 2.4 Hz, 3H), 4.21–4.16 (t, $J$ = 6.9 Hz, 6H), 3.56–3.52 (t, $J$ = 6.0 Hz, 6H), 1.95–1.92 (m, 24H), 1.76–1.75 (m, 6H), 1.50–1.40 (m, 6H), 1.26–1.10 (m, 12H), 1.07–1.00 (m, 36H), 0.89–0.82 (m, 24H), 0.80–0.59 (m, 54H), 0.50–0.45 (t, $J$ = 7.5 Hz, 18H). $^{13}$C NMR (CDCl$_3$, 75 MHz, ppm): δ 158.5, 152.1, 151.4, 150.6, 149.9, 141.8, 141.6, 140.6, 140.44, 140.37, 140.3, 139.8, 137.6, 131.5, 127.4, 127.0, 126.8, 125.8, 125.5, 125.3, 122.7, 122.6, 121.9, 121.0, 120.7, 120.6, 120.4, 120.2, 118.8, 118.6, 111.9, 109.3, 108.5, 67.3, 66.9, 55.0, 42.7, 40.5, 40.3, 31.2, 31.0, 29.7, 29.5, 29.0, 28.6, 26.9, 25.7, 23.7, 23.5, 22.4, 22.2, 14.0, 13.8. MALDI-TOF MS: Calcd for C$_{267}$H$_{285}$N$_3$O$_3$: 3583.23. Found: 3582.5 (M$^+$).

**FTaz**, white solid, (eluent: CH$_2$Cl$_2$–ethyl acetate = 4 : 1), (Yield: 70%): $^1$H NMR (CDCl$_3$, 300 MHz, ppm): δ 8.12–8.09 (d, $J$ = 7.8 Hz, 6H), 8.00 (s, 3H), 7.91 (s, 3H), 7.72–7.69 (d, $J$ = 6.9 Hz, 6H), 7.58 (s, 6H), 7.42 (s, 6H), 7.38–7.36 (d, $J$ = 6.9 Hz, 6H), 7.32–7.15 (m, 24H), 7.04–7.01 (d, $J$ = 7.5 Hz, 6H), 6.91–6.87 (m, 6H), 6.65–6.62 (d, $J$ = 8.4 Hz, 3H), 6.22–6.19 (dd, $J$ = 8.4 Hz, $J$ = 2.4 Hz, 3H), 6.10–6.09 (d, $J$ = 2.4 Hz, 3H), 4.07–4.02 (t, $J$ = 6.9 Hz, 6H), 3.60–3.56 (t, $J$ = 6.0 Hz, 6H), 1.95–1.92 (m, 24H), 1.79–1.75 (m, 6H), 1.49–1.40 (m, 6H), 1.26–1.19 (m, 12H), 1.07–1.00 (m, 36H), 0.89–0.82 (m, 24H), 0.80–0.60 (m, 54H), 0.52–0.47 (t, $J$ = 7.5 Hz, 18H). $^{13}$C NMR (CDCl$_3$, 75 MHz, ppm): δ 158.4, 152.1, 151.8, 151.4 150.6, 149.9, 142.7, 141.7, 141.5, 140.6, 140.5, 140.3, 139.8,

137.7, 131.5, 127.3, 127.0, 126.8, 125.7, 125.3, 125, 122.6, 121.8, 121.0, 120.7, 120.5, 120.2, 111.9, 109.3, 67.2, 66.9, 55.0, 49.4, 40.5, 40.3, 31.2, 31.0, 29.51, 29.49, 29.4, 28.9, 26.1, 25.4, 23.7, 23.5, 22.4, 22.2, 13.9, 13.7. MALDI-TOF MS: Calcd for C$_{237}$H$_{267}$N$_9$O$_3$: 3289.1. Found: 3288.7 (M$^+$).

**FOxd**, white solid, (eluent: CH$_2$Cl$_2$–ethyl acetate = 20 : 1), (Yield: 75%): $^1$H NMR (CDCl$_3$, 400 MHz, ppm): δ 8.13–8.11 (m, 12H), 8.03–8.01 (d, $J$ = 8.8 Hz, 6H), 7.70–7.69 (d, $J$ = 8.0 Hz, 6H), 7.72–7.69 (d, $J$ = 6.9 Hz, 6H), 7.57 (s, 6H), 7.54–7.52 (m, 12H), 7.42 (s, 6H), 7.29–7.27 (m, 6H), 7.24–7.17 (m, 24H), 7.03–7.01 (d, $J$ = 7.5 Hz, 6H), 6.95–6.92 (d, $J$ = 8.8 Hz, 6H), 6.90–6.86 (m, 6H), 6.63–6.61 (d, $J$ = 8.7 Hz, 3H), 6.22–6.20 (dd, $J$ = 8.7 Hz, $J$ = 2.4 Hz, 3H), 6.11–6.10 (d, $J$ = 2.4 Hz, 3H), 3.93–3.90 (t, $J$ = 6.4 Hz, 6H), 3.60–3.56 (t, $J$ = 6.1 Hz, 6H), 1.94–1.90 (m, 24H), 1.72–1.70 (m, 6H), 1.57–1.53 (m, 6H), 1.35–1.32 (m, 12H), 1.02–0.99 (m, 36H), 0.87–0.82 (m, 24H), 0.72–0.67 (m, 30H), 0.61–0.57 (m, 24H), 0.51–0.47 (t, $J$ = 7.5 Hz, 18H). $^{13}$C NMR (CDCl$_3$, 100 MHz, ppm): 164.6, 164.1, 161.9, 158.5, 152.1, 151.4, 150.6, 149.9, 141.8, 141.6, 140.6, 140.5, 140.3, 139.8, 137.7, 131.5, 129.0, 128.6, 127.4, 127.0, 126.8, 125.7, 124.1, 122.6, 121.9, 121.0, 120.7, 120.5, 120.2, 116.2, 114.9, 68.0, 67.4, 66.9, 55.0, 40.5, 40.3, 31.2, 31.0, 29.5, 29.46, 29.1, 28.9, 25.8, 23.7, 23.5, 22.4, 22.3, 13.9, 13.73. MALDI-TOF MS: Calcd for C$_{273}$H$_{288}$N$_6$O$_9$: 3796.23. Found: 3797.2 (M + H)$^+$.

## Acknowledgements

## References

1 (a) C. W. Tang and S. A. van Slyke, *Appl. Phys. Lett.*, 1987, **51**, 913–915; (b) J. H. Burroughes, D. D. C. Bradley, A. R. Brown, R. N. Marks, K. Mackay, R. H. Friend, P. L. Burns and A. B. Holmes, *Nature*, 1990, **347**, 539–541; (c) C. D. Muller, A. Falcou, N. Reckefuss, M. Rojahn, V. Wiederhirn, P. Rudati, H. Frohne, O. Nuyken, H. Becker and K. Meerholz, *Nature*, 2003, **421**, 829–833; (d) S. R. Forrest, *Nature*, 2004, **428**, 911–918.

2 S.-W. Wen, M.-T. Lee and C. H. Chen, *J. Display Technol.*, 2005, **1**, 90–99.

3 (a) A. Kraft, A. C. Grimsdale and A. B. Holmes, *Angew. Chem., Int. Ed.*, 1998, **37**, 402–428; (b) B. W. D'Andrade, M. E. Thompson and S. R. Forrest, *Adv. Mater.*, 2002, **14**, 147–151; (c) B. W. D'Andrade, J. Brooks, V. Adamovich, M. E. Thompson and S. R. Forrest, *Adv. Mater.*, 2002, **14**, 1032–1036; (d) Q. Zhang, Q. Zhou, Y. Cheng, L. Wang, D. Ma, X. Jing and F. Wang, *Adv. Mater.*, 2004, **16**, 432–436.

4 (a) W.-L. Yu, Y. Cao, J. Pei, W. Huang and A. J. Heeger, *Appl. Phys. Lett.*, 1999, **75**, 3270–3272; (b) D. Sainova, T. Miteva, H. G. Nothofer, U. Scherf, I. Glowacki, J. Ulanski, H. Fujikawa and D. Neher, *Appl. Phys. Lett.*, 2000, **76**, 1810–1812; (c) W.-L. Yu, J. Pei, W. Huang and A. J. Heeger, *Adv. Mater.*, 2000, **12**, 828–831; (d) X. Gong, P. K. Iyer, D. Moses, G. C. Bazan, A. J. Heeger and S. S. Xiao, *Adv. Funct. Mater.*, 2003, **13**, 325–330; (e) S. Tao, Z. Peng, X. Zhang, P. Wang, C.-S. Lee and S.-T. Lee, *Adv. Funct. Mater.*, 2005, **15**, 1716–1721; (f) Y. Jiang, L. Wang, Y. Zhou, Y.-X. Cui, J. Wang, Y. Cao and Jian Pei, *Chem.–Asian J.*, 2009, **4**, 548–553.

5 (a) V. N. Bliznyuk, S. A. Carter, J. C. Scott, G. Klarrner, R. D. Miller and D. C. Miller, *Macromolecules*, 1999, **32**, 361–369; (b) E. J. W. List, R. Guentner, P. S. de Freitas and U. Scherf, *Adv. Mater.*, 2002, **14**, 374–378; (c) L. Romaner,

A. Pogantsch, P. S. de Freitas, U. Scherf, M. Gaal, E. Zojer and E. J. W. List, *Adv. Funct. Mater.*, 2003, **13**, 597–601; (*d*) W. Zhao, T. Cao and J. M. White, *Adv. Funct. Mater.*, 2004, **14**, 783–790; (*e*) X.-H. Zhou, Y. Zhang, Y.-Q. Xie, Y. Cao and J. Pei, *Macromolecules*, 2006, **39**, 3830–3840.

6 (*a*) J. Luo, Y. Zhou, Z.-Q. Niu, Q.-F. Zhou, Y. Ma and J. Pei, *J. Am. Chem. Soc.*, 2007, **129**, 11314–11315; (*b*) J. Luo, T. Lei, X. Xu, F.-M. Li, Y. Ma, K. Wu and J. Pei, *Chem.–Eur. J.*, 2008, **14**, 3860–3865; (*c*) J. Luo, T. Lei, L. Wang, Y. Ma, Y. Cao, J. Wang and J. Pei, *J. Am. Chem. Soc.*, 2009, **131**, 2076–2077; (*d*) Z. Ning, Q. Zhang, H. Pei, J. Luan, C. Lu, Y. Cui and H. Tian, *J. Phys. Chem. C*, 2009, **113**, 10307–10313.

7 (*a*) J. M. Tour, R. Wu and J. S. Schumm, *J. Am. Chem. Soc.*, 1990, **112**, 5662–5663; (*b*) J. Guay, A. Diaz, R. Wu and J. M. Tour, *J. Am. Chem. Soc.*, 1993, **115**, 1869–1874.

8 (*a*) T. P. I. Saragi, T. Spehr, A. Siebert, T. Fuhrmann-Lieker and J. Salbeck, *Chem. Rev.*, 2007, **107**, 1011–1065; (*b*) R. Pudzich, T. Fuhrmann-Lieker and J. Salbeck, *Adv. Polym. Sci.*, 2006, **199**, 83–142; (*c*) J. Londenberg, T. P. I. Saragi, I. Suske and J. Salbeck, *Adv. Mater.*, 2007, **19**, 4049–4053.

9 (*a*) N. Cocherel, C. Poriel, J. Rault-Berthelot, F. Barrière, N. Audebrand, A. M. Z. Slawin and L. Vignau, *Chem.–Eur. J.*, 2008, **14**, 11328–11342; (*b*) C. Poriel, J.-J. Liang, J. Rault-Berthelot, F. Barrière, N. Cocherel, A. M. Z. Slawin, D. Horhant, M. Virboul, G. Alcaraz, N. Audebrand, L. Vignau, N. Huby, G. Wantz and L. Hirsch, *Chem.–Eur. J.*, 2007, **13**, 10055–10069; (*c*) Y. Wu, J. Zhang, Z. Fei and Z. Bo, *J. Am. Chem. Soc.*, 2008, **130**, 7192–7193; (*d*) Y. Wu, J. Li, Y. Fu and Z. Bo, *Org. Lett.*, 2004, **6**, 3485–3487.

10 (*a*) F.-I. Wu, D. S. Reddy, C.-F. Shu, M. S. Liu and A. K.-Y. Jen, *Chem. Mater.*, 2003, **15**, 269–274; (*b*) C. Ego, A. C. Grimsdale, F. Uckert, G. Yu, G. Srdanov and K. Mullen, *Adv. Mater.*, 2002, **14**, 809–811; (*c*) F. I. Wu, P. I. Shih, C. F. Shu, Y. L. Tung and Y. Chi, *Macromolecules*, 2005, **38**, 9028–9036.

11 (*a*) T. Miteva, A. Meisel, W. Knoll, H. G. Nothofer, U. Scherf, D. C. Müller, K. Meerholz, A. Yasuda and D. Neher, *Adv. Mater.*, 2001, **13**, 565–570; (*b*) M.-C. Hung, J.-L. Liao, S.-A. Chen, S.-H. Chen and A.-C. Su, *J. Am. Chem. Soc.*, 2005, **127**, 14576–14577; (*c*) Y. Jin, S. Song, J. Y. Kim, H. Kim, K. Lee and H. Suh, *Thin Solid Films*, 2008, **516**, 7373–7380.

12 (*a*) Y.-Z. Lee, X. Chen, S.-A. Chen, P.-K. Wei and W.-S. Fann, *J. Am. Chem. Soc.*, 2001, **123**, 2296–2307; (*b*) X. Chen, J.-L. Liao, Y. Liang, M. O. Ahmed, H.-E. Tseng and S.-A. Chen, *J. Am. Chem. Soc.*, 2003, **125**, 636–637; (*c*) C.-F. Shu, R. Dodda, F.-I. Wu, M. S. Liu and A. K.-Y. Jen, *Macromolecules*, 2003, **36**, 6698–6703; (*d*) C.-W. Huang, K.-Y. Peng, C.-Y. Liu, T.-H. Jen, N.-J. Yang and S.-A. Chen, *Adv. Mater.*, 2008, **20**, 3709–3716.

13 (*a*) J. Kido, K. Hongawa, K. Okuyama and K. Nagai, *Appl. Phys. Lett.*, 1993, **63**, 2627–2629; (*b*) J. Kido, M. Kimura and K. Nagai, *Science*, 1995, **267**, 1332–1334; (*c*) L. S. Yu and S.-A. Chen, *Adv. Mater.*, 2004, **16**, 744–748.

14 Z.-L. Wei, P. A. Petukhov, F. Bizik, J. C. Teixeira, M. Mercola, E. A. Volpe, R. I. Glazer, T. M. Willson and A. P. Kozikowski, *J. Am. Chem. Soc.*, 2004, **126**, 16714–16715.

15 Joseph R. Lakowicz, in *Principles of Fluorescence Spectroscopy*, Plenum Publishing Corporation, 2nd edn, 1999.

16 S. Janietz and A. Wedel, *Adv. Mater.*, 1997, **9**, 403–407.

17 (*a*) F. Huang, L. T. Hou, H. B. Wu, X. H. Wang, H. L. Shen, W. Cao, W. Yang and Y. Cao, *J. Am. Chem. Soc.*, 2004, **126**, 9845–9853; (*b*) J. Kido, H. Shionoya and K. Nagai, *Appl. Phys. Lett.*, 1995, **67**, 2281–2283.

18 (*a*) Q. Hou, Q. M. Zhou, Y. Zhang, W. Yang, R. Q. Yang and Y. Cao, *Macromolecules*, 2004, **37**, 6299–6305; (*b*) X. Gong, M. R. Robinson, J. C. Ostrowski, D. Moses, G. C. Bazan and A. J. Heeger, *Adv. Mater.*, 2002, **14**, 581–585; (*c*) L. Wang, Y. Jiang, J. Luo, Y. Zhou, J. Zhou, J. Wang, J. Pei and Y. Cao, *Adv. Mater.*, 2009, **21**, 4854–4858.

19 C. Y. Kwong, A. B. Djuriić, V. A. L. Roy, P. T. Lai and W. K. Chan, *Thin Solid Films*, 2004, **458**, 281–286.